Xu Q, Hu Z, Jiang Z.

Experimental investigation of sloshing effect on the hydrodynamic responses of an FLNG system during side-by-side operation.

***Ships and Offshore Structures* 2017**

Experimental investigation of sloshing effect on the hydrodynamic responses of an FLNG system during side-by-side operation

Qiaowei Xu[a], Zhiqiang Hu[a,b], Zhe Jiang[c]

a. State Key Laboratory of Ocean Engineering, Shanghai Jiao Tong University, Shanghai, China

b. School of Marine Science and Technology, Newcastle University, Newcastle upon Tyne, UK

c. Hadal Science and Technology Research Center, Shanghai Ocean University, Shanghai, China

Abstract: This study experimentally examined the effect of sloshing on the hydrodynamic responses of FLNG (floating liquefied natural gas) systems during side-by-side operation. Decay, white noise and irregular wave tests with wind and current were conducted. To determine the influence of sloshing, the vessels were ballasted with solid and liquid cargo. Wave probes were installed in the tanks to determine the free surface elevation. The results show that sloshing has a pronounced effect on the roll motion and the relative sway motion. During side-by-side operation under this liquid ballast conditions, the ranges of the roll motion and the relative sway motion were reduced. The maximum tension on the hawsers or fenders and the collision frequency of the fenders also decreased. These results indicate that under this liquid loading condition, sloshing can have a beneficial effect on the motions and the induced loads of the connected system. This information will be helpful for carrying out the numerical calculation and also for optimising the operation of FLNG systems.

Keywords: FLNG; hydrodynamics; sloshing effect; side-by-side operation; free surface oscillation

1. Introduction

With the growing demand for offshore natural gas exploration, FLNG systems have emerged as a new type of platform for offshore natural gas production. Traditionally for near-shore natural gas exploration, natural gas is transported to an onshore terminal by pipelines. However, this option becomes less attractive because the cost of pipeline transportation increases dramatically with increasing water depth and distance from the coastline. An FLNG system can liquefy the natural gas and transport it using a liquefied natural gas carrier (LNGC), which provides a viable option for deep-water natural gas production. One of the technical challenges for FLNG production systems is the offloading operation of the liquefied natural gas (LNG) to the LNGC. Due to the cryogenic properties of the LNG, the offloading arms can't be set too long. As a consequence, the preferred option for offloading practices is the side-by-side operation. During side-by-side operation, the FLNG and LNGC are aligned and connected by hawsers and fenders to maintain a specified relative distance. The hydrodynamic responses of the two vessels during offloading operation have profound influences on the feasibility of FLNG systems.

Hydrodynamic responses of FLNG and LNGC systems during offloading operation are dependent on many factors such as metocean conditions and the proximity effect of the two

vessels. It has been found that the sloshing of LNG in the vessels' compartments and the gap flow between the vessels also affects the hydrodynamic performance of the vessels. When interior and exterior liquid flow resonance occurs, the motion of the vessels may be more evident. Sloshing can decrease the motion range for example, with an anti-rolling tank, but sloshing can also increase the motion range under other circumstances. Whether this sloshing phenomenon has a positive or negative effect on offloading operation is still an unanswered question far from common agreement. Thus, it is essential to determine the effect of sloshing on vessel motion.

Many studies have been performed regarding the sloshing effect of liquid in a tank. Molin et al. (2002) and Malenica et al. (2003) used linear analyses to study the coupled tank/ship motion. Faltisen et al. (2011) constructed an accurate analytical approximation of the natural sloshing modes in a rectangular tank with a slat-type screen at the tank middle using the linear sloshing theory and domain decomposition method. Lee et al. (2007) simulated the temporal effect of liquid sloshing using a Navier-Stokes solution and applied the sloshing force and moment as external excitations to the ship's motion, which was in turn used as the input excitation for liquid sloshing. Kim et al. (2007) compared two numerical methods, the finite-difference method and the smoothed-particle-hydrodynamics (SPH) method, to investigate the strongly nonlinear sloshing flows, which verified that the nonlinearity of the sloshing-induced forces and moments plays a critical role in the coupling effect. Lee et al. (2015) performed nonlinear response in FLNG cargo tank structures under sloshing loads with ANSYS/LS-DYNA nonlinear finite element software. Paik et al. (2015) determined the sloshing loads during the structural design of LNG FPSO with a new probabilistic approach.

The sloshing effect of the gap flow between the vessels is one of the moonpool problems. Molin et al. (2001) used linearized potential flow theory to determine the natural modes of oscillation of the free surfaces between vessels in two and three dimensions. Liu et al. (2014) gave a semi-analytical solution for gap resonance between two fixed, partially immersed rectangular boxes based on linear potential theory. Feng et al. (2015) and Kristiansen et al. (2010) performed a mixed Eulerian-Lagrangian scheme by a higher-order boundary element method to express the nonlinear free surface boundary condition and studied the wave resonance in a narrow gap. Kristiansen et al. (2013) used a hybrid method combing potential and viscous flow to present a 3D moonpool where the free-surface motion is governed by potential theory and a Navier-Stokes solver provides the solution in the main bulk of the water.

Experimental studies regarding sloshing and hydrodynamic interference effect have also been performed. Nasar et al. (2008) studied sloshing in different filled tanks mounted on a barge exposed to regular beam waves and the study primarily investigated the effect of the wave excitation frequency and wave elevation on the sloshing oscillation and on the response of the barge. Berg et al. (2008) performed model tests in the MARINTEK basin and compared two ways of offloading operations: side-by-side and tandem configurations. However, these two sets of model tests greatly simplified the tank and the vessel, making the results unsuitable for representing the true hydrodynamic characteristics of FLNG and LNGC systems. Zhao analysed the influence of internal sloshing on the hydrodynamics of an FLNG system (Zhao et al. 2013) and hydrodynamic interaction between FLNG and LNGC systems (Zhao et al. 2012). However, in his test, the effect of sloshing on an FLNG system during side-by-side operation was not researched adequately. The wave elevation in the FLNG tank was not considered.

Since sloshing is a typical problem with strong nonlinear hydrodynamics, its theory requires

further improvement. Moreover, the accuracy of numerical results should be verified. Although model tests have scale effects, they can reflect the impact of sloshing on the hydrodynamics of an FLNG system with satisfactory accuracy. The sloshing effect on the hydrodynamic performance of an FLNG system during side-by-side operation was experimentally investigated in this study. The FLNG and LNGC were ballasted with solid and liquid contents. Only the two-dimensional sloshing effects in shallow liquid depths were considered. The purpose of this study was to clarify the following issues:

(1) The coupling effect between the vessels' motions and sloshing in the tanks;
(2) The motions and the induced loads of the FLNG system during side-by-side offloading operation;
(3) The motions of the free surface in the tanks.

It should be pointed out that in this study, only one typical loading combination that showing serious sloshing effect, was chosen for the two vessels, because the primary goal was to investigate the sloshing effect on side-by-side offloading operation. The hydrodynamic characteristics are closely related to the loading combinations of the two vessels, although this factor is not considered in this paper. Additional research on this topic will be performed in the future.

2. Description of the FLNG system

2.1 Features of the FLNG and the LNGC

The model test was conducted at a scale ratio of 1:60. The FLNG facilities are designed to serve at a site with a water depth of 1500 m and are equipped with 10 identical LNG tanks that are arranged in two columns. The LNGC is equipped with 4 LNG tanks in one column. The FLNG under 75% loading condition and the LNGC under 70% loading condition were selected. This loading combination is the most common situation and both the two vessels have enough liquid in their tanks. The motion range of the vessels is evident in this loading combination. The parameters of the FLNG and the LNGC under liquid conditions are similar to those under solid conditions. The distance between the FLNG and the LNGC is 5.8m. Wave probes were installed in the No. 1 and NO. 5 LNG tank of the FLNG and the NO. 3 LNG tank of the LNGC as shown in Fig. 4. The main parameters of the two vessels are shown in Table 1, and those of the tanks in the vessels are shown in Table 2. The photo of the tank and the wave probes is also shown in Fig. 1.

Fig. 1 Photo of the tank with installed wave probes.

Table 1 Principal parameters of the FLNG and the LNGC.

Designation	Symbol	Unit	FLNG	LNGC

			Prototype	Model	Prototype	Model
Length overall	Loa	m	340	5.67	214.2	3.57
Breadth	B	m	61	1.02	31.8	0.53
Depth	D	m	37	0.62	19.20	0.32
Draft	d	m	16.80	0.28	7.52	0.13
Displacement	Δ	ton	302,237	1.40	38,500	0.18
Centre of gravity above base	KG	m	22.60	0.38	10.50	0.18
Centre of gravity from AP	XG	m	161.98	2.70	102.34	1.71
Radius of pitch gyration	Ryy	m	85.21	1.42	63.06	1.05

Table 2 Principal parameters of the tanks.

Design ation	Symb ol	Unit	FLNG		LNGC	
			Prototype	Model	Prototype	Model
Length	L	m	37.0	0.617	49.2	0.82
Width	B	m	26.4	0.44	25.2	0.42
Height	H	m	30.9	0.515	15.6	0.26

2.2 Features of the turret-mooring system

The FLNG platform is moored by 18 3600-m-long mooring lines that are attached to an internal turret. The mooring system consists of three bundles that are spread (120°) in a circle; the separation angle between the neighbouring lines in the same bundle is 5°. Each line is composed of three segments (chain-wire-chain) and has a horizontal span of 3148.9 m. The pre-tension on the top of each mooring line is 5000 kN. The positions of the mooring lines are shown in Fig. 2.

Considering the limitations of available artificial water basins, the mooring system is truncated (Stansberg et al. 2000, Su et al. 2009) to a prototype water depth of 350 m. Because the truncated system is not the focus of this research, it is not described in detail in this paper.

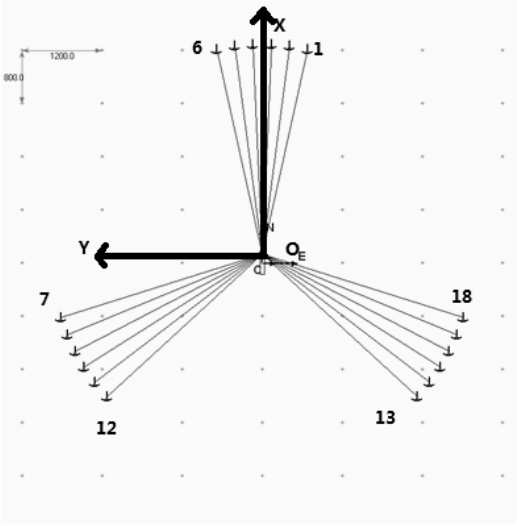

Fig. 2 Arrangement of the mooring lines.

2.3 Features of the side-by-side arrangement

The FLNG and the LNGC are connected by 8 hawsers and 4 fenders (see Fig. 4). The hawsers are numbered from #1 to #8, and the fenders are numbered from #9 to #12. Fig. 3 shows the configuration of the model tests. The characteristics of the hawsers are listed in Table 3. The nonlinear characteristics of the fenders are shown in Fig. 5.

Fig. 3 Configuration of the FLNG and the LNGC during side-by-side operation.

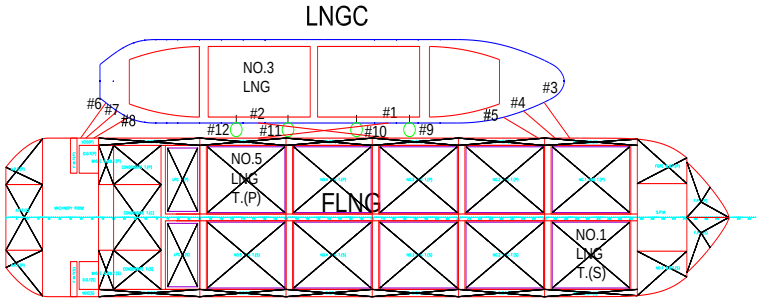

Fig. 4 Configuration of the side-by-side arrangement.

Table 3 Configuration of the hawsers.

Quantity	Diameter (mm)	Length (m)	Breaking load (kg)	Stiffness (N/m)
6	96	18	221,400	100,450
2	96	60	221,400	100,450

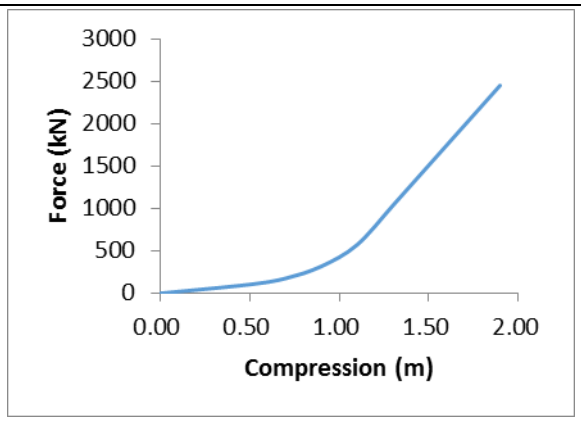

Fig. 5 Nonlinear force-compression relationship of the fenders.

2.4 Environmental conditions

Marine environmental conditions can vary widely during offloading operation and relatively harsh conditions are common. In this study, the one-year return sea condition is selected. The random wave component is described by a three-parameter JONSWAP spectrum with a significant wave height of 6.2 m, a peak period of 11.1 s and a peak enhancement factor of 2.0. The velocity of the wind and the current are 19.3 m/s and 1.05 m/s respectively. The directions of the wave, wind and current are 180 degree. Case 1 (solid condition) and Case 2 (liquid condition) are selected.

3 Test results and discussion

The model tests included decay tests in still water, white noise tests and irregular wave tests with wind and current. A comparison of the experimental data measured under both solid and liquid ballast conditions was made.

3.1 Natural period

When the FLNG system is under side-by-side operation condition, both the liquid in the tanks and the gap flow between the vessels have the sloshing effect. The interior and exterior liquid flow resonances may occur. As a consequence, whether the natural periods of the interior and exterior liquid flow are close to each other should be considered. Fig. 6 shows the parameters of the natural period function of the interior and exterior liquid flow.

3.1.1 The natural period of the interior liquid flow

The natural period T_n of the interior liquid in each tank is expressed as follows (Lee et al. 2008):

$$T_n = \frac{2\sqrt{\pi B}}{\sqrt{ng\tanh(\frac{n\pi h}{B})}} \quad , \ \text{n=1,2,3…,} \tag{1}$$

where B is the breadth or the length of the tanks, g denotes gravitational acceleration, h indicates the water depth and n represents the surface mode number.

3.1.2 The natural period of the exterior liquid flow

The natural period T_0 of the exterior liquid flow between the vessels is expressed as follows (Molin et al. 2001):

$$T_0 = \frac{\sqrt{g}}{\sqrt{H + (b/\pi) \times \left(\frac{3}{2} + \ln(\frac{L}{2b})\right)}} \tag{2}$$

where b is the width of the gap between the vessels, g denotes gravitational acceleration, H stands for the draught of the vessel and L represents the total width of the two vessels.

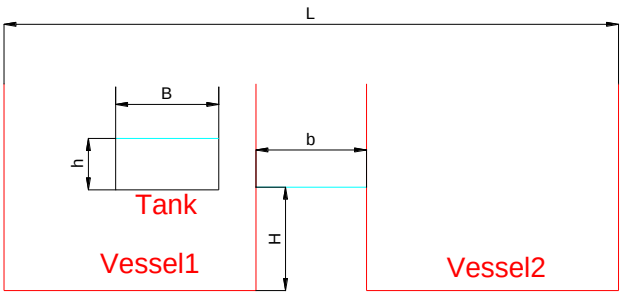

Fig 6 The parameters of the natural periods function of the interior and exterior liquid flow.

3.1.3 The comparison of the natural periods of the interior and exterior liquid flow

The possible draught of the FLNG ranges from 15m to 18m and the natural period of the exterior liquid flow varies from 9.35s to 9.97s, which are shown in Table 4. Likewise, the height of the liquid in the tanks changes from 14m to 32m and the natural period of the interior liquid flow varies from 6.03s to 5.82s. It is indicated that the natural periods of the interior and exterior liquid flow are quite different and it is hard for the resonance to occur. As a consequence, among

the most common situations, the FLNG under 75% loading condition and the LNGC under 70% loading condition are selected as the reference loading condition combination. The natural periods of the interior and exterior liquid flow are shown in Table 5.

Table 4 The natural periods of the interior and exterior liquid flow of different liquid height.

The height of the liquid in the tanks(m)	14.0	17.0	20.0	23.0	26.0	29.0	32.0
The natural period of the interior liquid(s)	6.03	5.92	5.87	5.84	5.83	5.82	5.82
The draught of the vessel(m)	15.0	15.5	16.0	16.5	17.0	17.5	18.0
The natural period of the exterior liquid(s)	9.35	9.46	9.56	9.67	9.77	9.87	9.97

Table 5 The natural periods of the interior and exterior liquid under the reference condition.

	Transverse natural period		Longitudinal natural period	
Interior liquid flow	1st:5.84	2nd: 4.11	1st: 7.02	2nd: 4.87
Exterior liquid flow	9.73	-	-	-

3.2 Sloshing effect on the natural period

In decay tests, vessels with solid and liquid compartments respond under transient excitation. The statistical results are presented in Table 6. The time histories of the FLNG under the 75% loading condition are shown in Fig. 7.

Table 6 Decay statistical results for the FLNG under 75% loading condition.

Loading condition	Ballast	Period (s)			Damping coefficient		
		Roll	Pitch	Heave	Roll	Pitch	Heave
75%	Solid	23.95	11.53	11.87	0.0122	0.1269	0.1513
75%	Liquid	25.88	11.64	11.85	0.0248	0.118	0.1467

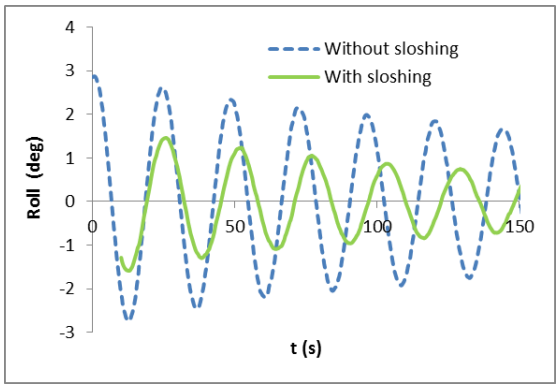

(a) Roll decay curve

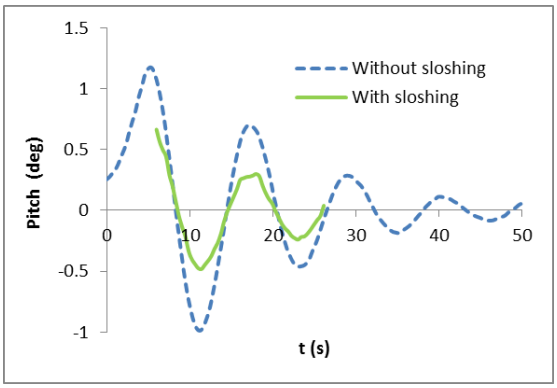

(b) Pitch decay curve

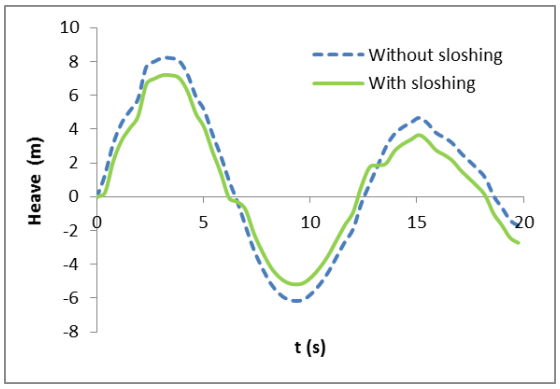

(c) Heave decay curve

Fig. 7 Decay curves for the FLNG under the 75% loading condition.

Fig. 7 and Table 6 show that the influence of sloshing differs under different motion modes. Sloshing has a significant impact on the roll motion and less of an influence on the pitch motion and heave motion. The natural period and damping coefficient of the roll motion under liquid condition is higher than that under solid condition. This is because the motion phase angles of the free surface in the tanks and the FLNG are quite different. The natural period of the pitch under liquid condition is slightly amplified while the damping coefficient is nearly the same. This is because the longitudinal inertia radius of the FLNG is much greater than the transverse inertia radius so that the effect on the pitch appears small. Little difference in the heave motion is also observed. This is because the liquid is moving up and down with the vessel, which can be regarded as a solid mass.

3.3 Sloshing effect on RAO

During the white noise sea tests, the responses of the six-degree-of-freedom motions for the single FLNG with and without sloshing were determined, and the response amplitude operator (RAO) was calculated. As the RAO curves for the low-frequency motions of the FLNG under different ballast conditions are nearly the same, only the RAO curves for the wave-frequency motions are presented. The RAO curves for the wave-frequency motions under different wave directions are compared in Fig. 8.

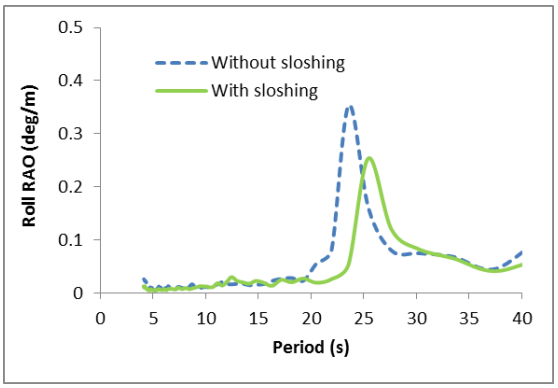

(a) RAO curve for the roll at 180 degrees

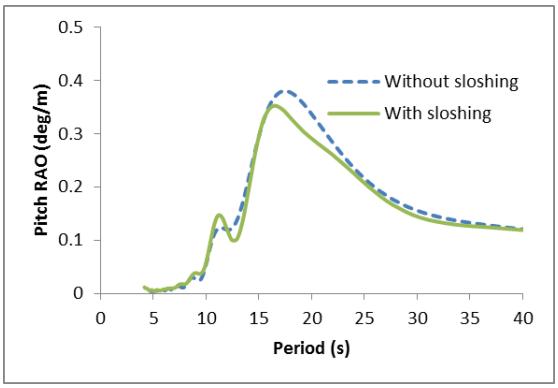

(b) RAO curve for the pitch at 180 degrees

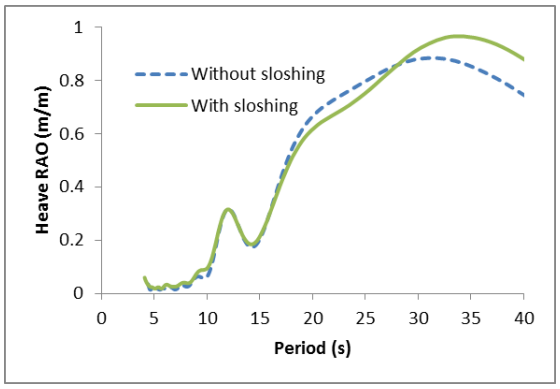

(c) RAO curve for the heave at 180 degrees

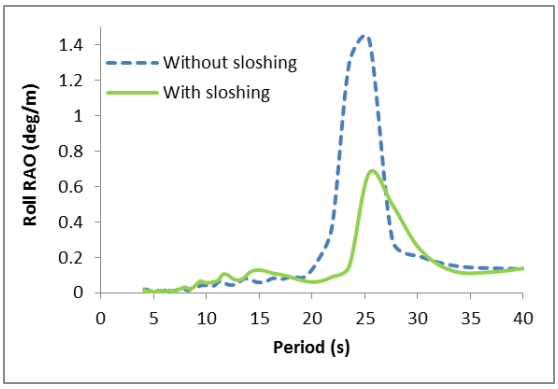

(d) RAO curve for the roll at 150 degrees

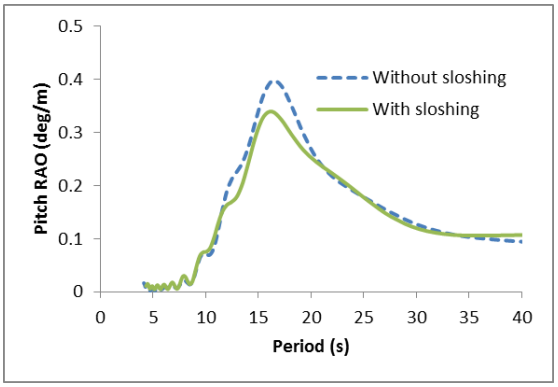

(e) RAO curve for the pitch at 150 degrees

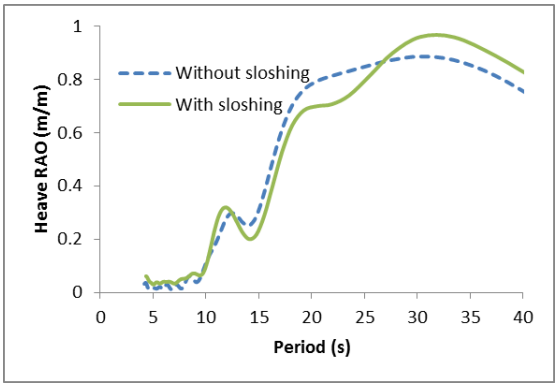

(f) RAO curve for the heave at 150 degrees

Fig. 8 RAO curves for the wave-frequency motions of the FLNG with and without sloshing under the 75% loading condition under wave directions of 180 degrees and 150 degrees.

It is shown in Fig. 8 that although the tendency of RAO curves for the wave-frequency motions with and without sloshing show a good agreement, there are some differences between the RAO curves under different ballast conditions. The RAO curves for the roll motion of the vessel under solid and liquid condition are significantly different. The peak resonance period of the FLNG under liquid condition shifts from 24 s to 26 s, which is consistent with the observation from the decay test results. Furthermore, the peak value decreases, and the phenomenon is much more obvious for a wave direction of 150 degrees. The coupling effect creates a secondary peak at a shorter period, which is not as significant as that when the FLNG is at higher filling condition. These results are consistent with the observations of Gou et al. (2011).

It is also indicated in Fig. 8 (b) and Fig. 8 (e) that the RAO curve for the pitch motion is slightly affected by the sloshing because the longitudinal inertia radius of the FLNG is sufficiently large to inhibit the sloshing effect. The RAO curve for the heave of the FLNG does not exhibit evident changes either. This phenomenon is also supported by the decay test results.

3.4 Sloshing effect on the motion of vessels and loads on connecting system

3.4.1 Motions characteristics of the FLNG and the LNGC

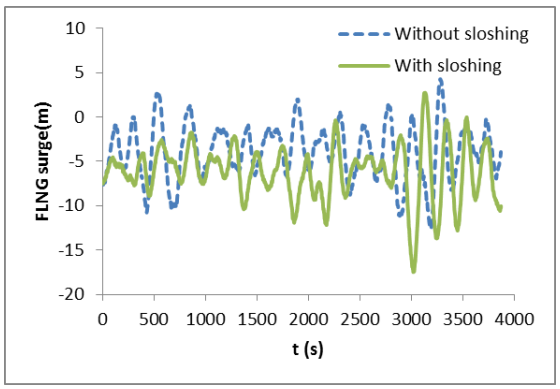

(a) FLNG surge

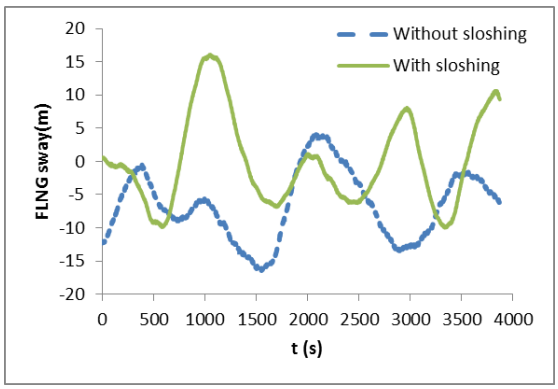

(b) FLNG sway

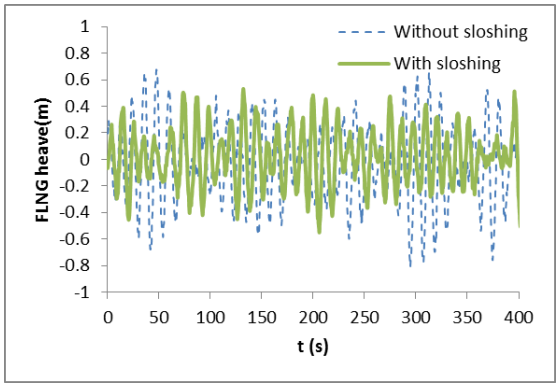

(c) FLNG heave

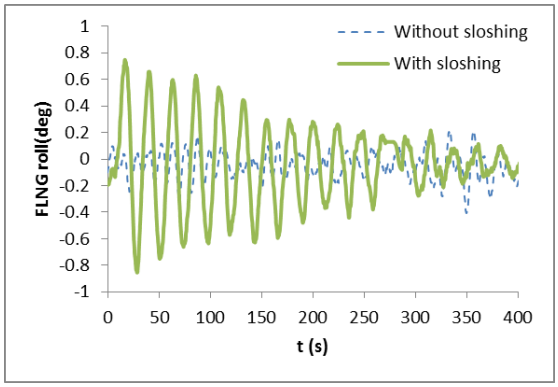

(d) FLNG roll

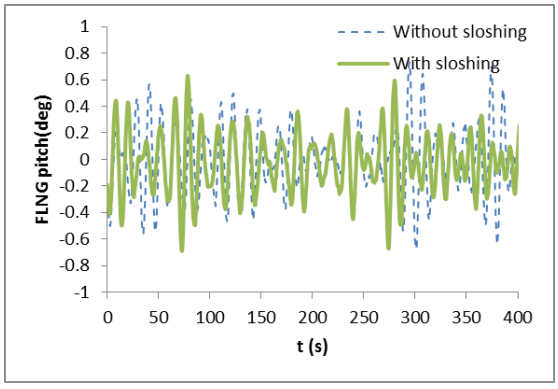

(e) FLNG pitch

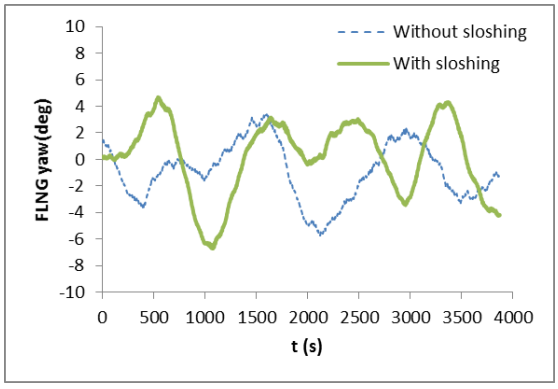

(f) FLNG yaw

Fig. 9 Motion response of the FLNG.

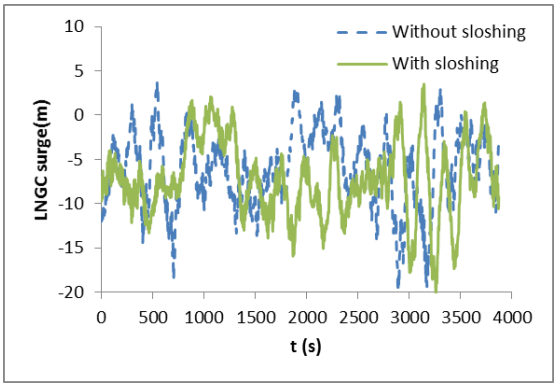

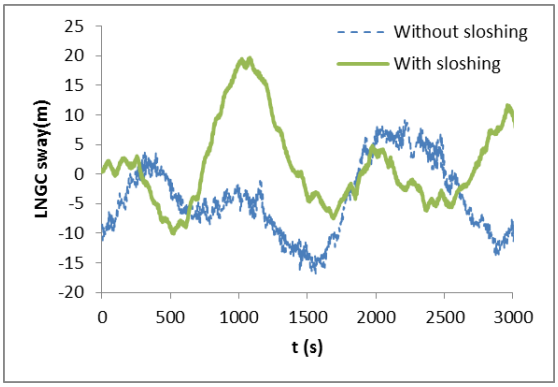

(a) LNGC surge

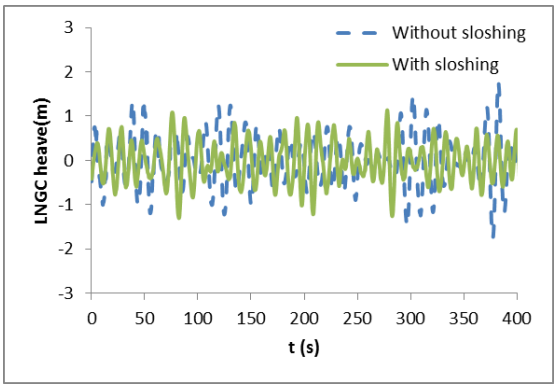

(b) LNGC sway

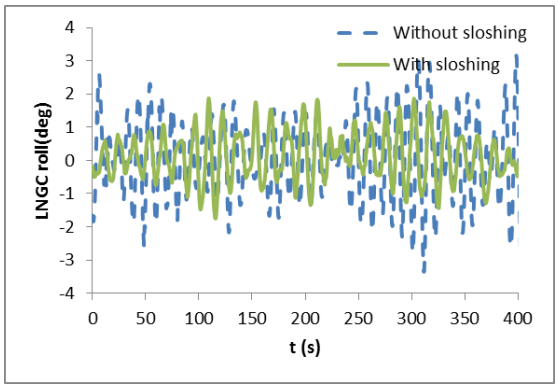

(c) LNGC heave

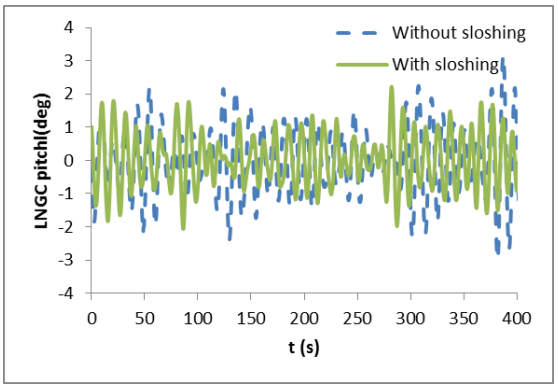

(d) LNGC roll

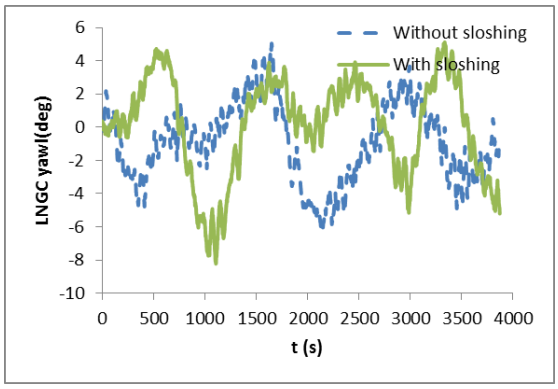

(e) LNGC pitch

(f) LNGC yaw

Fig. 10 Motion response of the LNGC.

Table 7 Statistical results for the motions of the FLNG and the LNGC under solid and liquid condition.

Loading condition		Solid				Liquid			
Motion	Unit	Max	Min	Mean	Amp	Max	Min	Mean	Amp
FLNG surge	m	4.31	-12.65	-3.82	16.96	2.74	-17.49	-6.22	20.23
FLNG sway	m	4.07	-16.42	-6.56	20.48	16.10	-10.00	0.06	26.10
FLNG heave	m	0.83	-0.88	-0.03	1.71	0.90	-0.86	-0.01	1.77
FLNG roll	deg	0.75	-0.85	-0.05	1.60	0.35	-0.54	-0.09	0.89
FLNG pitch	deg	0.75	-0.76	-0.01	1.51	0.82	-0.79	-0.02	1.61
FLNG yaw	deg	3.38	-5.76	-0.93	9.14	4.69	-6.72	0.17	11.42
LNGC surge	m	3.83	-20.05	-5.91	23.87	3.51	-20.11	-7.21	23.63
LNGC sway	m	9.07	-16.87	-3.78	25.94	19.69	-10.15	1.60	29.84
LNGC heave	m	1.83	-1.74	0.00	3.57	1.67	-1.57	-0.03	3.23
LNGC roll	deg	4.59	-4.12	0.09	8.71	3.57	-3.17	0.07	6.74
LNGC pitch	deg	3.34	-3.32	-0.03	6.65	3.23	-2.97	0.04	6.20
LNGC yaw	deg	5.07	-6.20	-0.89	11.28	5.12	-8.23	0.10	13.35

Typical time series of the motions of the FLNG and the LNGC are shown in Fig. 9 and Fig. 10, respectively. The statistical results of the motions are listed in Table 7. Amp in this table means the amplitude of the motions, which means the maximum value minus the minimum value. Regardless of the ballast conditions, the LNGC has larger amplitude motions than those of the

FLNG (Table 7) due to the large displacement and inertia of the FLNG. Moreover, the coupling interactions between the FLNG and the LNGC increase the motion amplitudes of the LNGC to a certain extent.

The sloshing effect on the FLNG motions features well with that on the LNGC motions. It is shown in Fig. 9 (d) and Fig. 10 (d) that when the vessels are under liquid condition, the roll amplitude is small. The roll amplitude of the LNGC is reduced by approximately 2 degree, which is a 25% reduction, whereas that of the FLNG is reduced by 0.7 degree, which is even a 50% reduction. Therefore, the FLNG exhibits a larger reduction in the roll amplitude. This is because the FLNG possesses two tanks for every row while the LNGC possesses one tank for every row and the width of different tanks in different vessels is nearly the same.

The pitch amplitudes are slightly higher under liquid condition as shown in Table 7, which can be explained by the motions of the free surface (Section 3.4.4). In addition, the heave motions of the vessels under different conditions are nearly the same. These results are consistent with the decay test results and the white noise test results.

As shown in Table 7, the amplitudes of the low-frequency motions of the FLNG and the LNGC under liquid condition are higher than those under solid condition. This indicates that the linear motions of the vessels increase, which is of great importance because the relative low-frequency motions may cause the offloading arms to carry more substantial loads. The time histories and the spectra for the relative low-frequency motions are shown in Fig. 11, and the statistical results are presented in Table 8. The relative motions are determined from the motions of the LNGC minus the motions of the FLNG.

Table 8 Statistical results for the relative motions.

Loading condition		Solid				Liquid			
Motion	Unit	Max	Min	Mean	Amp	Max	Min	Mean	Amp
Relative surge	m	3.97	-10.40	-2.38	14.37	6.89	-6.98	-0.35	13.87
Relative sway	m	10.22	-2.20	2.76	12.42	4.61	-1.23	0.54	5.84
Relative yaw	deg	2.75	-2.45	0.06	5.20	1.63	-2.22	-0.03	3.86

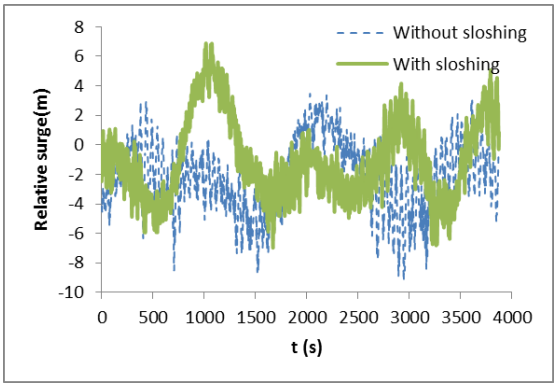

(a) Relative surge

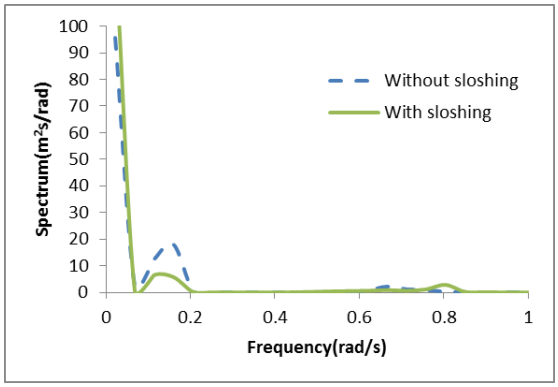

(b) Relative surge spectrum

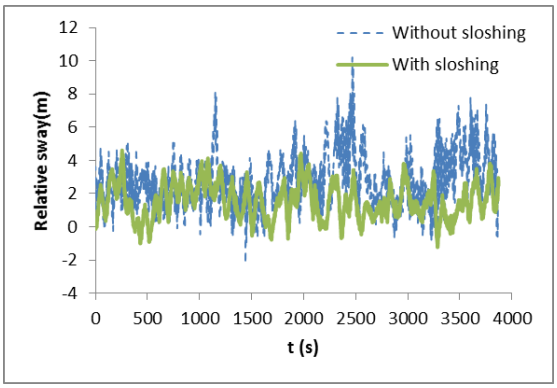

(c) Relative sway

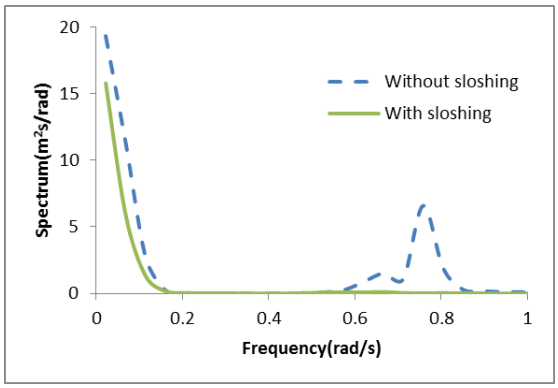

(d) Relative sway spectrum

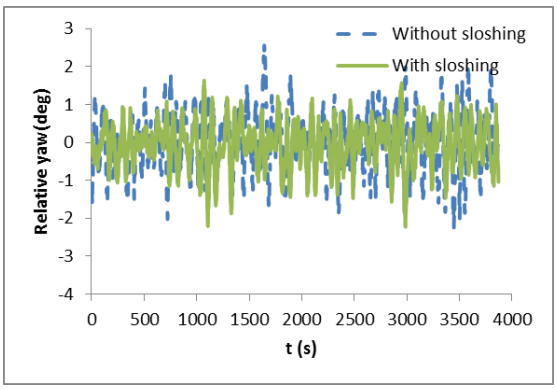

(e) Relative yaw

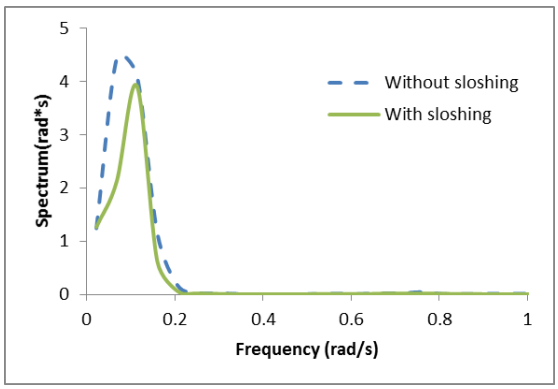

(f) Relative yaw spectrum

Fig. 11 Time histories and spectra for the relative motions.

The relative motions consist of wave-frequency and low-frequency motions; and all of the relative motions have a prominent low-frequency component (Fig. 11). This characteristic was also observed by Kim et al. (2012). Compared with the relative sway, the relative surge has a significant low-frequency component (Fig. 11(b)) and larger amplitude variations (Table 8), which may induce large loads on the connecting system. The relative sway has a significant wave-frequency component (Fig. 11(d)), which is likely to cause structural damage to the connected system due to fatigue.

The amplitude of the relative surge under liquid condition is slightly higher than that under solid condition; the mean value of the relative surge approaches zero, and the maximum value decreases (Table 8.). It is indicated that the relative surge fluctuates around zero and may reduce the force on the connected system. There is a significant reduction in the amplitude of the relative sway (Table 8). However, as shown in Table 7, the sway amplitudes of both the FLNG and the LNGC increase. This may be caused by the phase angle between the sway motions of the two vessels. Fig. 11(f) shows that the relative yaw spectra for the different loading conditions are nearly the same, and Table 8 shows that the amplitudes of the relative yaw are consistent. It can be concluded that the relative yaw is only slightly affected by sloshing. The spectra in Fig. 11 show that under this loading combination, sloshing can reduce the wave-frequency motions of the relative surge and the relative sway.

3.4.2 Characteristics of loads on the hawsers

The loads on the hawsers are affected by the relative motions, particularly the relative surge and

the relative sway. Hawser #1 represents hawsers in the middle of the vessels, and Hawser #5 represents hawsers at the fore and aft of the vessels (Hawser #3-Hawser #8). The relative surge and the loads on Hawser #1 and Hawser #5 are shown in Fig. 12, and the relative sway and the loads on Hawser #1 and Hawser #5 are shown in Fig. 13.

The pattern of the loads on Hawser #1 is similar to that of the relative surge and sway. Fig. 12 shows that when the relative surge and sway increase, the loads on Hawser #1 increase, which means that the loads on the hawsers in the middle of the vessels are affected by the relative surge and sway. The pattern of the loads on Hawser #5 is different from that of the relative surge but similar to that of the relative sway. It can be concluded that the loads on the hawsers at the fore and aft of the vessels are primarily affected by the relative sway.

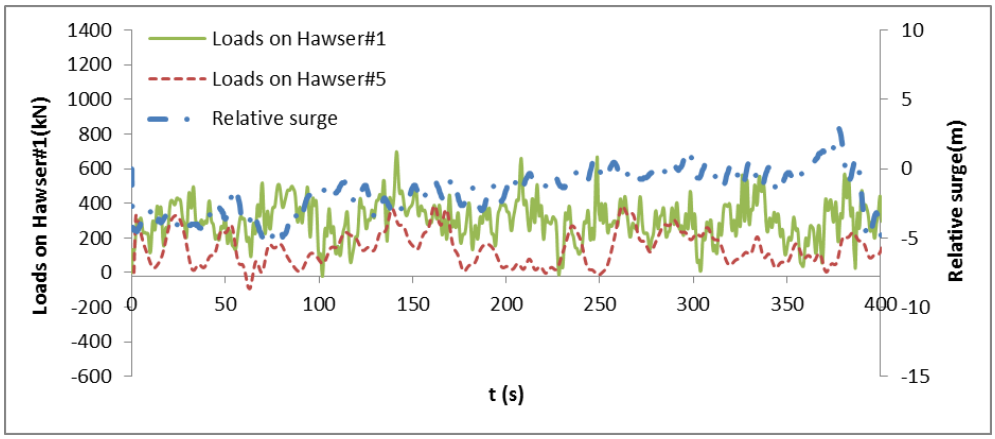

Fig. 12 The relative surge and the loads on Hawser #1 and Hawser #5 under liquid condition.

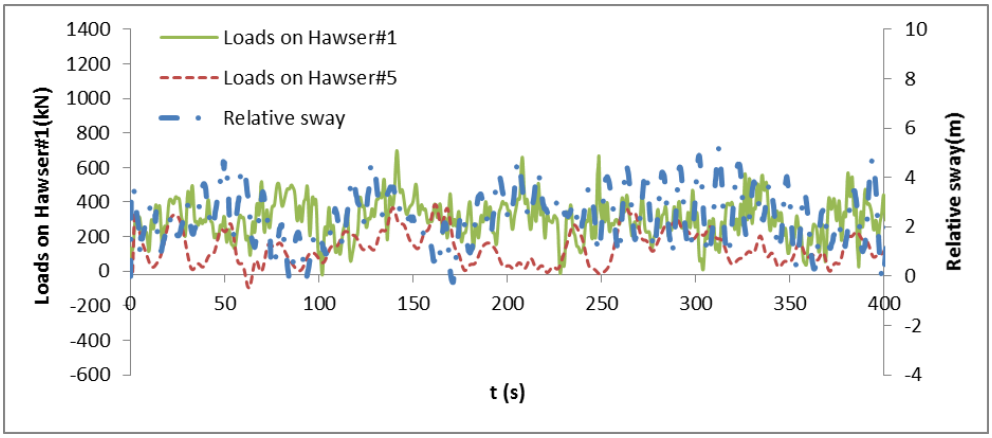

Fig. 13 The relative sway and the loads on Hawser #1 and Hawser #5 under liquid condition.

The statistical results for the loads on the hawsers are shown in Table 9, in which negative values mean that the tension is less than the initial value. The time histories and spectra of the loads on the Hawser #1 and Hawser #2 are shown in Fig. 14. The results in Table 9 show that when the vessels are under liquid condition, the maximum and mean loads on all of the hawsers are lower except for Hawser #1. Because the loads on the hawsers at the fore and aft of the vessels are primarily affected by the relative sway whose extreme value and mean value decrease under liquid conditions. The loads on Hawser #1 become greater while the loads on Hawser #2 get smaller. It should be noted that Hawser #1 bears the loads from the aft and Hawser #2 bears the loads from the fore. Under the liquid conditions, the relative surge becomes more positive, which means the loads from the aft become larger and loads from the fore become smaller. As a result,

Hawser #1 should be reinforced to resist the higher tensions caused by sloshing.

Table 9 Loads on the hawsers.

Loading condition		Solid			Liquid		
No.	Unit	Max	Min	Mean	Max	Min	Mean
Hawser #1	kN	803	-328	241	1,106	-345	308
Hawser #2	kN	1,072	-118	477	859	42	447
Hawser #3	kN	982	-67	246	801	-177	185
Hawser #4	kN	1,011	-89	334	749	-32	264
Hawser #5	kN	913	-175	221	648	-93	160
Hawser #6	kN	733	-148	114	511	-234	62
Hawser #7	kN	650	-109	115	350	-84	90
Hawser #8	kN	663	-129	137	432	-166	117

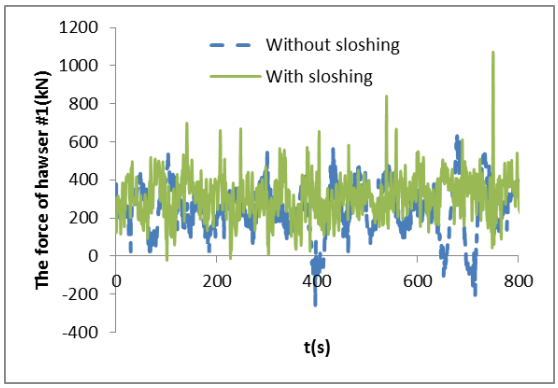

(a) Time history for the loads on Hawser #1

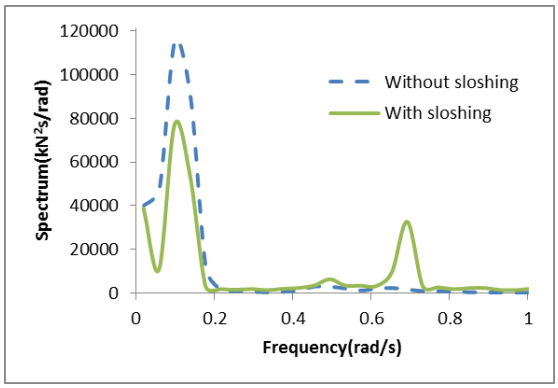

(b) Spectrum curves for the loads on Hawser #1

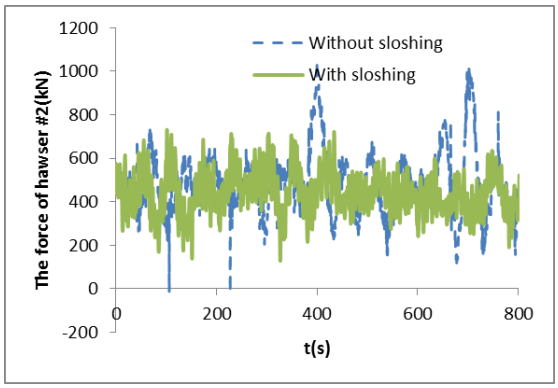

(c) Time history for the loads on Hawser #2

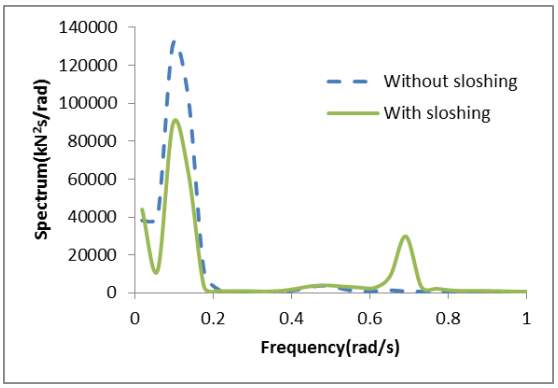

(d) Spectrum curves for the loads on Hawser #2

Fig. 14 Time histories and PSD curves for the loads on Hawser #1 and Hawser #2.

The PSD curves in Fig. 14 demonstrate that the loads on the hawsers can be decomposed into two parts: wave-frequency loads and low-frequency loads. Sloshing can increase the wave-frequency loads and also decrease the low-frequency loads, which is quite different from the sloshing effect on the relative linear motions of vessels. The wave-frequency loads may be primarily caused by the relative angular motions of vessels. This phenomenon may cause hawsers to be damaged by fatigue, which should be carefully monitored.

3.4.3 Characteristics of loads on the fenders

The statistical results of the loads on the fenders are shown in Table 10, in which negative values indicate pressure, whereas positive values indicate that the pressure is less than the initial value. The time histories for the loads on the fenders are given in Fig. 15. The results in Table 10 demonstrate that the maximum loads on the fenders decrease because they are related to the minimum relative sway, which is lower under liquid conditions.

Table 10 Loads on the fenders.

Loading condition		Solid			Liquid		
No.	Unit	Max	Min	Mean	Max	Min	Mean
Fender #9	kN	532	-2,134	332	463	-1,637	364
Fender #10	kN	234	-1,303	-10	160	-465	49
Fender #11	kN	319	-844	129	220	-105	133
Fender #12	kN	298	-2,114	105	328	-1,607	172

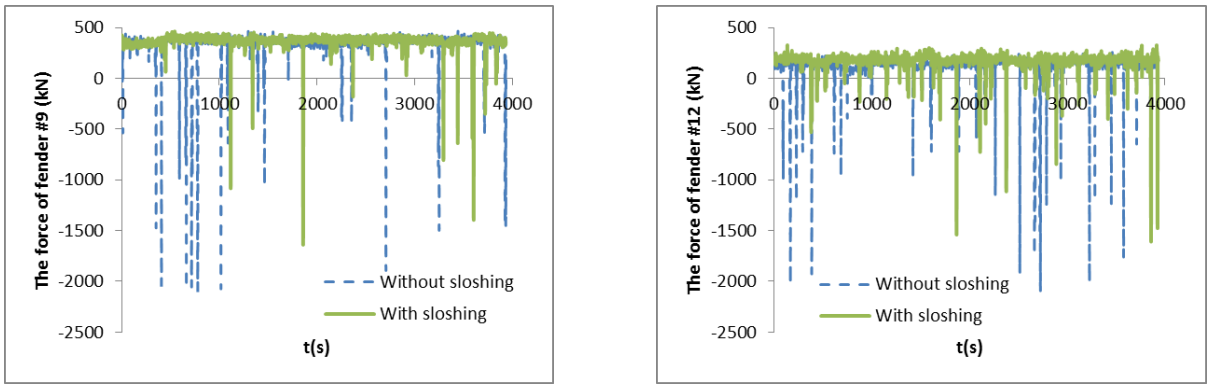

(a) Force on Fender #9

(b) Force on Fender #12

Fig. 15 Time histories of the forces on Fender #9 and Fender #12.

Table 11 Number of collision for various fenders under different conditions.

Loading condition	Solid				Liquid			
Fender	Fender	Fender	Fender	Fender	Fender	Fender	Fender	Fender
Number	#9	#10	#11	#12	#9	#10	#11	#12
Collision number	68	0	1	77	16	0	0	26

The number of collisions on the fenders is presented in Table 11. Fig. 15 and Table 11 show that the number of collisions between fenders decreases under liquid conditions because sloshing reduces the wave-frequency relative motions. The number of collisions for Fender #12 is greater than for Fender #9 because Fender #12 is at the end of the FLNG, which is affected by the relative sway and relative yaw. Consequently, the aft portion of the FLNG has more pronounced motions than the forward portion of the FLNG. In contrast, the maximum pressures on Fender #12 and Fender #9 are nearly the same, verifying the conclusion that the forces on the fenders are primarily affected by the relative sway.

3.4.4 Characteristics of motions of the free surface

During side-by-side offloading operation, the FLNG and the LNGC systems always contain LNG in their compartments, and sloshing affects the hydrodynamic performance of a single vessel and the coupled hydrodynamics of multiple bodies. Thus, this paper is focused on the interaction

between the motions of the free surface and the motions of vessels based on time histories.

Kim et al. (2011) found that in the case of a 56% filled tank, the free surface moves according to an almost straight line. The size of the tanks used was similar to the size of those used for the FLNG in this work. Consequently, the free surface of the FLNG can be considered to move as a linear surface, and violent free-surface motions, such as overturning and splash, are not considered in this paper.

The motion of the free surface in the transverse direction is defined as the roll of the free surface, and the motion in the longitudinal direction is defined as the pitch of the free surface. Taking the roll in Fig. 16 as an example, the extent of the roll is given by

$$\alpha = \arctan[(h_2 - h_1)/a] \tag{3}$$

where *h1* and *h2* denote the wave elevations obtained by the wave probes in the transverse direction, *a* indicates the distance between the wave probes in the transverse direction, and α is the extent of the roll. The definition for the pitch of the free surface is similar to that of the roll.

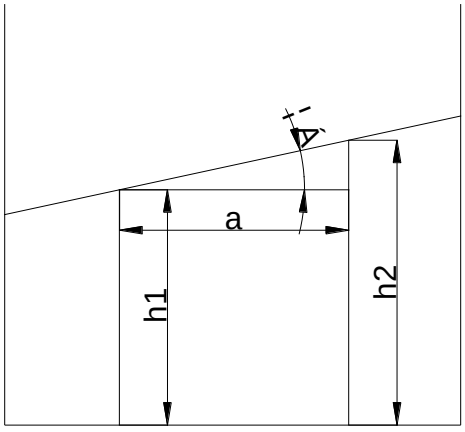

Fig. 16 The definition for the roll of the free surface.

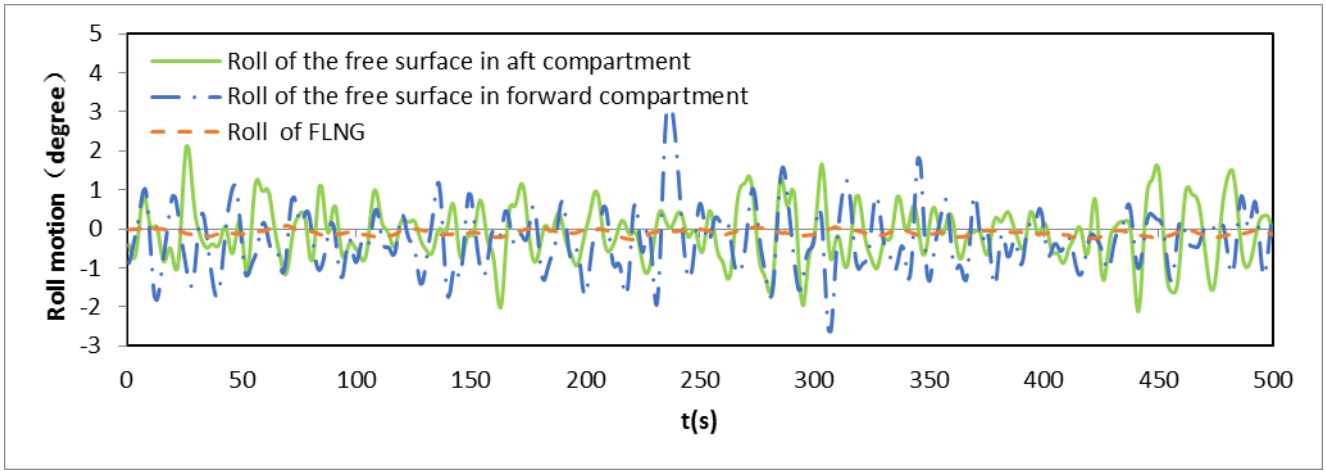

Fig. 17 The roll of the FLNG and the free surface.

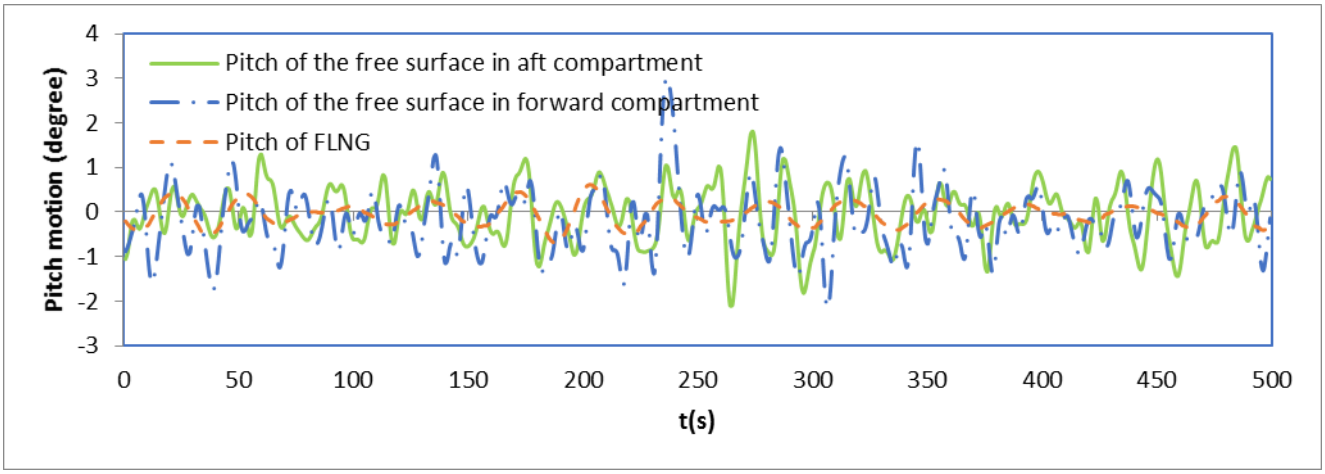

Fig. 18 The pitch of the FLNG and the free surface.

The roll and pitch of the FLNG and the free surface in different compartments are depicted in Fig. 17 and Fig. 18, respectively. The statistical results for the motions are listed in Table 12. As shown in Fig. 17 and Fig. 18, the amplitudes of the free surface motions are much larger than the motion amplitudes of the FLNG, especially for the roll motion amplitudes. The roll phases of the free surface are different from the roll phases of the FLNG, while the pitch phases of the free surface are similar to the pitch phases of the FLNG. This finding can explain why the roll amplitude of the FLNG decreases and the pitch amplitude of the FLNG increases, which was discussed in Section 3.4.1. Fig. 17 and Fig. 18 also show that the phase angles of the free surface in the aft compartment and the forward compartment are consistent.

Table 12 shows that the roll amplitude of the free surface in the aft compartment is greater than that in the forward compartment because the roll of the free surface is sensitive to the roll and yaw motion of the FLNG and the aft portion of the FLNG experiences larger motions. In contrast, the pitch amplitudes of the free surface motion in the different compartments are nearly the same, which may be because the centre of gravity of the FLNG is located at approximately the middle of the vessel.

Table 12 Statistical results for the motions of the FLNG and the free surface.

	Roll			Pitch		
	FLNG	Aft compartment	Forward compartment	FLNG	Aft compartment	Forward compartment
Max	0.35	3.35	3.29	0.82	2.85	3.00
Min	-0.54	-4.40	-3.03	-0.79	-2.58	-2.20
Mean	-0.09	-0.09	-0.25	-0.02	-0.02	-0.14
Amp	0.89	7.75	6.32	1.61	5.44	5.20

4 Conclusions

The side-by-side offloading operation of an FLNG with an LNGC was modelled in this study. The FLNG and the LNGC systems were ballasted with solid and liquid cargo to allow for a comparative analysis of the effect of sloshing on hydrodynamic performance. The main conclusions are as follows:

(1) Sloshing has a beneficial effect on FLNG motion for certain loading combinations. Sloshing has the greatest impact on the roll period and peak value.

(2) The relative motions between the two vessels are composed of wave-frequency motion and

low-frequency motion. Sloshing can reduce the range of relative motions and the wave-frequency components of the relative motions under certain circumstances.

(3) The loads on the hawsers can be decomposed into low-frequency loads and wave-frequency loads. Sloshing increases the wave-frequency loads and decreases the low-frequency loads. The maximum loads on the hawsers and fenders and the frequency of fender collisions are lower for vessels under liquid ballast condition.

(4) For the FLNG, the roll amplitude for the internal free surface in the aft compartment is greater than that in the forward compartment while the pitch amplitudes are the same. The phase angles of the free surface motion in the aft compartment and the forward compartments are consistent.

(5) In this paper, no numerical results are shown, which will be made for comparison in the future. Besides, only one typical loading combination was chosen for the two vessels. However, the hydrodynamic characteristics are closely related to the loading combinations of the two vessels. Additional research on this loading combination will be performed in future work.

Acknowledgments

The authors gratefully acknowledge financial support from a China National Scientific and Technology Major Project (Grant No. 2011ZX05026-006-05), and the State Key Laboratory of Hydraulic Engineering Simulation and Safety, Tianjin University (Grant No. HESS-1404).

References

Berg TE, Bakke J. 2008. Ship-to-ship LNG transfer in arctic waters, Proceedings of the 27th International Conference on Offshore Mechanics and Arctic Engineering. Estoril, Portugal, OMAE. OMAE2008-57319.

Faltinsen OM, Timokha AN. 2011. Natural sloshing frequencies and modes in a rectangular tank with a slat-type screen. Journal of Sound and Vibration. 330(7): 1490-1503.

Feng X, Bai W. 2015. Wave resonances in a narrow gap between two barges using fully nonlinear numerical simulation. Applied Ocean Research. 50: 119-129.

Gou Y, Kim Y, Kim TY. 2011. A numerical study on coupling between ship motions and sloshing in frequency and time domains. The Twenty-first International Offshore and Polar Engineering Conference. International Society of Offshore and Polar Engineers.

Kim MH, Lee BH, Hwang SC, Park JC. 2011. Sloshing Effect on Multi-Vessel Motions by Using Moving Particle Simulation. The Twenty-first International Offshore and Polar Engineering Conference. International Society of Offshore and Polar Engineers.

Kim MS, Jeong HS, Kwak HW, Kim BW, Eom JK. 2012. Improvement method on offloading operability of side-by-side moored FLNG. The Twenty-second International Offshore and Polar Engineering Conference. International Society of Offshore and Polar Engineers.

Kim Y. 2007. Experimental and numerical analyses of sloshing flows. Journal of Engineering Mathematics. 58(1-4): 191-210.

Kristiansen T, Faltinsen OM. 2010. A two-dimensional numerical and experimental study of resonant coupled ship and piston-mode motion. Applied Ocean Research. 32(2): 158-176.

Kristiansen T, Sauder T, Firoozkoohi R. 2013. Validation of a hybrid code combining potential and viscous flow with application to 3D moonpool. ASME 2013 32nd International Conference on Ocean, Offshore and Arctic Engineering. American Society of Mechanical Engineers. V009T12A029-V009T12A029.

Lee SE, Kim BJ, Seo JK, Ha YC, Matsumoto T, Byeon SH, Paik JK. 2015. Nonlinear impact response analysis of LNG FPSO cargo tank structures under sloshing loads. Ships and Offshore Structures. 10(5): 510-532.

Lee SJ, Kim MH, Lee DH, Kim JW, Kim YH. 2007. The effect of LNG-tank sloshing on the global motions of LNG carriers. Ocean Eng. 34(1): 10-20.

Lee SJ. 2008. The effect of LNG-sloshing on the global responses of LNG-carriers. Texas A&M University.

Liu Y, Li HJ. 2014. A new semi-analytical solution for gap resonance between twin rectangular boxes. Proceedings of the Institution of Mechanical Engineers, Part M: Journal of Engineering for the Maritime Environment. 228(1): 3-16.

Malenica S, Zalar M, Chen XB. 2003. Dynamic coupling of seakeeping and sloshing. 13th International Offshore and Polar Engineering Conference, ISOPE, Honolulu, HI, May. 25-30.

Molin B, Remy F, Rigaud S, de Jouette Ch. 2002. 'LNG-FPSO's: frequency domain, coupled analysis of support and liquid cargo motions. IMAM Conf, Rethymnon, Greece.

Molin B. 2001. On the piston and sloshing modes in moonpools. Journal of Fluid Mechanics. 430: 27-50.

Nasar T, Sannasiraj SA, Sundar V. 2008. Experimental study of liquid sloshing dynamics in a barge carrying tank. Fluid Dynamics Research. 40(6): 427-458.

Paik JK, Lee SE, Kim BJ, Seo JK, Ha YC, Matsumoto T and Byeon SH. 2015. Toward a probabilistic approach to determine nominal values of tank sloshing loads in structural design of liquefied natural gas FPSOs, Journal of Offshore Mechanics and Arctic Engineering, Vol.137, 021801-1 - 021801-17.

Stansberg CT, Yttervik R, Øritsland O, Kleiven G. 2000. Hydrodynamic model test verification of a floating platform system in 3000 m water depth. Proceedings of 19th International Conference on Offshore Mechanics and Arctic Engineering, New Orleans, LA, USA. OMAE2000-4145.

Su YH, Yang JM, Xiao LF, Chen G. 2009. Experimental and numerical study on large truncation of deepwater mooring line. Proceedings of the 28th International Conference on Offshore Mechanics and Arctic Engineering. Honolulu, Hawaii, USA. OMAE 2009-79218.

Zhao WH, Yang JM, Hu ZQ. 2013. Effects of sloshing on the global motion responses of FLNG. Ships and Offshore Structures. 8(2): 111-122.

Zhao WH, Yang JM, Hu ZQ. 2012. Hydrodynamic interaction between FLNG vessel and LNG carrier in side by side configuration. Journal of Hydrodynamics, Ser. B. 24(5): 648-657.